Analysis of Frequency Selective Surface on Isotropic/Anisotropic Layers Using WCIP Method

Mohammed Titaouine, Alfrêdo Gomes Neto, Henry Baudrand, and Farid Djahli

The wave concept iterative procedure (WCIP) is used to analyze arbitrarily shaped frequency selective surfaces (FSS). The WCIP method is developed from the fast modal transform based on a two-dimensional fast Fourier transform algorithm. Using the proposed procedure, less computing time and memory are needed to calculate the scattering parameters of the FSS structure. The method is applied to the modeling of an FSS structure of a rectangular patch and a comparison with experimental results confirms good agreement.

Keywords: Frequency selective surface (FSS), wave concept iterative procedure (WCIP), fast modal transform (FMT).

Manuscript received May 04, 2006; revised Sept. 20, 2006.

Mohammed Titaouine (email: m.titaouine@caramail.com) is with Institute d'Electronique, Centre Universitaire de Bordj Bou, Arréridj, Algeria.

Alfrêdo Gomes Neto (email: T.Arslan@ed.ac.uk) is with Telecommunication and Electromagnetisme Group, Federal Education Technological Center of Paraiba, João Pessoa, Brazil.

Henry Baudrand (email: henribaudrand@laposte.net) is with the Ecole Supérieure d'Electronique Electrotechnique Informatique, ENSEEIHT, Toulouse, France.

Farid Djahli (email: f.djahli@yahoo.fr) is with the Electronics Institute, University of Sétif, Sétif, Algeria.

I. Introduction

Frequency selective surfaces (FSSs) find widespread applications as spatial filters for antenna and infrared applications and so on [1], [2]. The analysis of the FSS structures can be carried out by the immittance approach in conjunction with the method of moments [3]. Even though the latter approach provides good results, the WCIP method offers two major advantages, namely, simplicity of use and no limitation on the form of the patch. Moreover, a very important gain in computation time is obtained by the use of the two-dimensional fast Fourier transform (FFT) algorithm [4].

The proposed method is able to characterize FSS structures of arbitrarily shaped patches deposited on multilayer isotropic/anisotropic dielectrics and is based upon a multiple reflection procedure. In this method, an FSS is considered as a periodic structure where the unit cell is analyzed independently to give the characteristics of the overall FSS structure. Analysis using the WCIP is carried out via two major steps which are repeated until convergence is reached. The two steps include scattering of the normal incident wave at the interface, characterized by the presence of the metallic patch in the spatial domain, and reflection from the closing ends of the box in which the unit cell can be hypothetically contained. Each mode reflected from the closing ends is characterized by a given reflection coefficient. Hence, a decomposition of the wave at the periodic wall as guide modes (transverse electromagnetic, TEM; transverse electric, TE; and transverse magnetic, TM modes) should take place by the use of the fast modal transform (FMT). The inverse FMT is adopted to return to the spatial domain. The procedure is repeated until convergence is obtained.

The FSSs of rectangular patches deposited on two isotropic/anisotropic dielectric layers are considered for the

different substrate parameters of cell and patch dimensions. Good agreement is observed when the obtained results are compared to published experimental and simulated results.

II. Theory

The FSS shown in Fig.1 consists of a periodic array of arbitrarily shaped patches deposited on a multilayer uniaxial anisotropic substrate. The permittivity tensor $\bar{\varepsilon}_i$ of the *i*-th dielectric layer is given by [5]

$$\bar{\varepsilon}_i = \varepsilon_0 \begin{bmatrix} \varepsilon_{xxi} & 0 & 0 \\ 0 & \varepsilon_{yyi} & 0 \\ 0 & 0 & \varepsilon_{zzi} \end{bmatrix}, \quad (1)$$

where *i* designates the layer number from 2 to *n*.

In the WCIP method, the FSS is seen as a periodic structure and its analysis is reduced to the analysis of the repeated structure, the unit cell. The periodic walls, represented by dashed lines in Fig. 1, are assumed to separate adjacent cells. Figure 2(a) represents the unit cell to be analyzed.

The WCIP is based on a transverse wave's formulation. For the N-layer FSS shown in Fig. 2(b), the analysis is reduced to the case of the two-media wave problem illustrated in Fig. 3.

The incident waves $\vec{A}_i$ and the scattered waves $\vec{B}_i$ are given in terms of the transverse electric and magnetic fields at the interface as [6]

$$\begin{aligned} \vec{A}_i &= \frac{1}{2\sqrt{Z_{0i}}}\left(\vec{E}_{Ti} + Z_{0i}\left(\vec{H}_{Ti} \wedge \vec{n}\right)\right) \\ \vec{B}_i &= \frac{1}{2\sqrt{Z_{0i}}}\left(\vec{E}_{Ti} - Z_{0i}\left(\vec{H}_{Ti} \wedge \vec{n}\right)\right), \end{aligned} \quad (2)$$

where *i* indicates the medium 1 or 2, Z_{oi} stands for the characteristic impedance of the same medium, and $\vec{n}$ is the outward vector normal to the interface.

For the sake of simplicity, the surface current density is introduced as

$$\vec{J}_i = \vec{H}_{Ti} \wedge \vec{n}. \quad (3)$$

From (2) and (3), the transverse waves $\vec{A}_i^{(k)}$ and $\vec{B}_i^{(k)}$ can be used to calculate the tangential electric fields and the current intensity on each of the two sides of the interface as

$$\begin{aligned} \vec{E}_i &= \sqrt{Z_{oi}}\left(\vec{A}_i + \vec{B}_i\right) \\ \vec{J}_i &= \frac{1}{\sqrt{Z_{oi}}}\left(\vec{A}_i - \vec{B}_i\right). \end{aligned} \quad (4)$$

At the *k*-th iteration, the incident waves $\vec{A}_i^{(k)}$ are scattered by the interface to give rise to the waves $\vec{B}_i^{(k)}$. They are

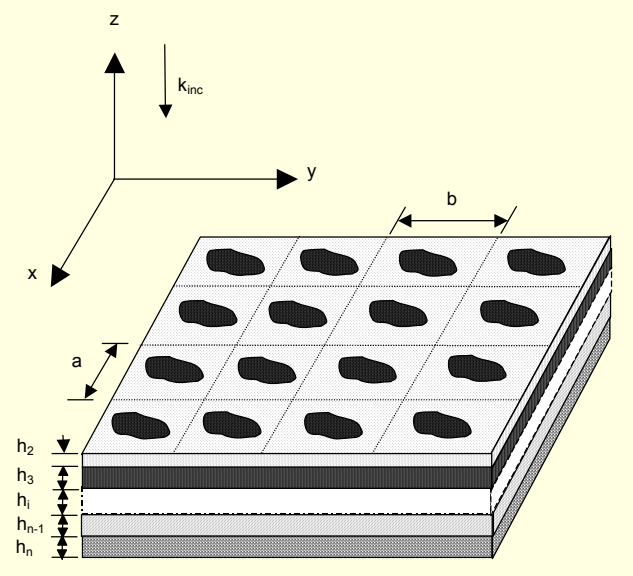

Fig. 1. Geometry of arbitrarily shaped FSS on n multilayer substrate with normal incidence.

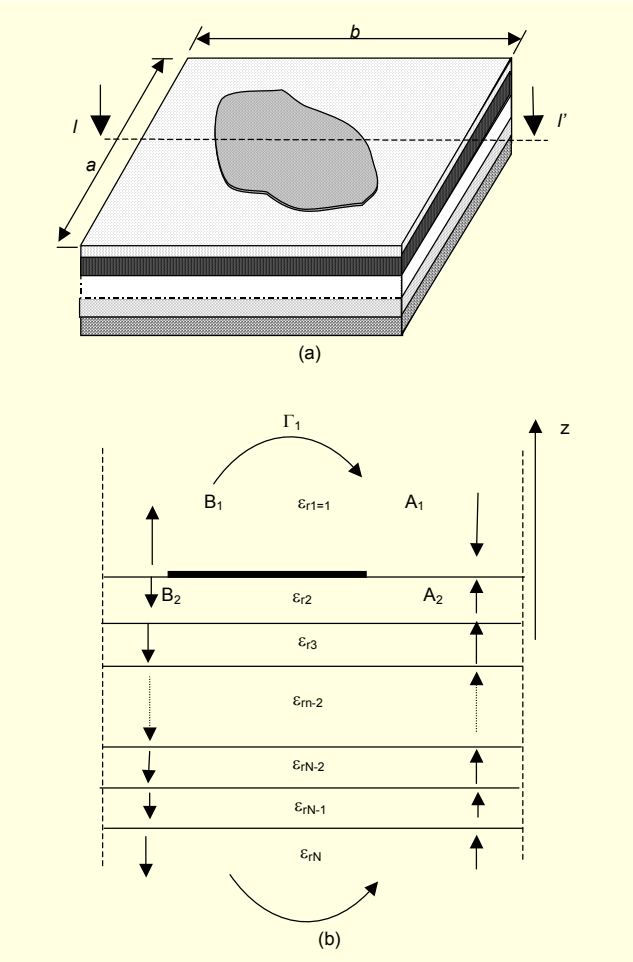

Fig. 2. (a) The unit cell in the FSS structure and (b) a section of unit cell along ll' axis.

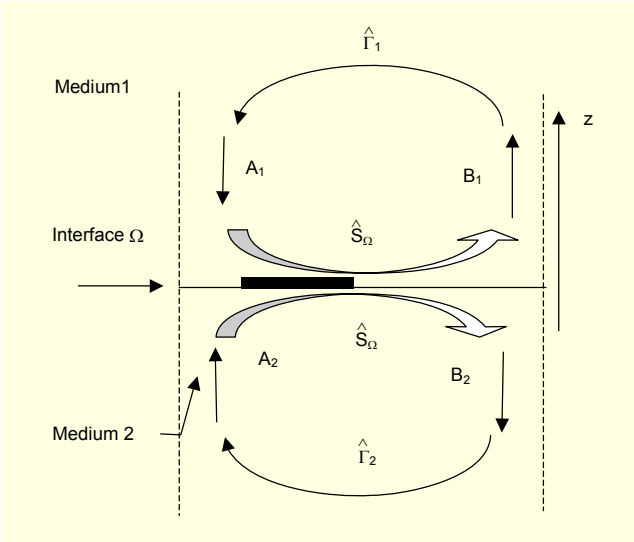

Fig. 3. Two-media problem as seen by the WCIP.

related by

$$\vec{B}_i^{(k)} = \hat{S}_\Omega \vec{A}_i^{(k)}. \tag{5}$$

A scattering operator, $\hat{S}_\Omega$, is defined in the spatial domain and accounts for the boundary conditions.

The scattered waves $\vec{B}_i^{(k)}$ will be reflected to generate the new incident waves to which the incident source waves are to be added as

$$\vec{A}_i^{(k+1)} = \hat{\Gamma}_i B_i^{(k)} + \vec{A}_0, \tag{6}$$

where $\vec{A}_0$ denotes the incident source waves and $\hat{\Gamma}_i$ is the reflection operator which is defined in the spectral domain.

1. Scattering Operator Determination

The interface domain consists of two sub-domains: a dielectric domain H_I and a metal domain H_M. Using the boundary conditions of each domain, the scattering operator $\hat{S}_\Omega$ can be determined.

A. Metal Domain Scattering Operator $\hat{S}_M$

On this part of the interface the tangential electric field is canceled on both media. The boundary conditions of this domain are given by

$$\vec{E_1} = \vec{E_2} = \vec{0}. \tag{7}$$

Substituting (4) into (7) results in

$$\sqrt{Z_{o1}}\left(\vec{A}_1 + \vec{B}_1\right) = \sqrt{Z_{o2}}\left(\vec{A}_2 + \vec{B}_2\right) = \vec{0}, \tag{8}$$

which gives

$$\begin{cases} \vec{B}_1 = -\vec{A}_1 \\ \vec{B}_2 = -\vec{A}_2 \end{cases} \Rightarrow \begin{vmatrix} \vec{B}_1 \\ \vec{B}_2 \end{vmatrix} = \begin{vmatrix} -1 & 0 \\ 0 & -1 \end{vmatrix} \begin{vmatrix} \vec{A}_1 \\ \vec{A}_2 \end{vmatrix}. \tag{9}$$

The metal domain scattering operator $\hat{S}_M$ is given in terms of the metallic domain generator H_M by

$$\left[\hat{S}_M\right] = \begin{vmatrix} -H_M & 0 \\ 0 & -H_M \end{vmatrix}. \tag{10}$$

H_m is a Heaviside unit step defined as

$$H_M = \begin{cases} 1, & \text{on the metal,} \\ 0, & \text{otherwise.} \end{cases}$$

B. Dielectric Domain Scattering Operator $\hat{S}_I$

The boundary conditions on a dielectric domain are given as

$$\begin{cases} \vec{J}_{tot} = \vec{J}_1 + \vec{J}_2 = \vec{0}, \\ \vec{E}_1 = \vec{E}_2. \end{cases} \tag{11}$$

Taking (4) and replacing it into (11), the scattered waves $\vec{B}_i$ are found to be related to the incident waves $\vec{A}_i$ as

$$\begin{vmatrix} \vec{B}_1 \\ \vec{B}_2 \end{vmatrix} = \begin{vmatrix} \frac{1-N^2}{1+N^2} & \frac{2}{1+N^2} \\ \frac{2}{1+N^2} & -\frac{1-N^2}{1+N^2} \end{vmatrix} \begin{vmatrix} \vec{A}_1 \\ \vec{A}_2 \end{vmatrix} \tag{12}$$

with

$$N = \sqrt{\frac{Z_{o1}}{Z_{o2}}}. \tag{13}$$

The dielectric domain scattering operator $\hat{S}_I$ is given in terms of the dielectric domain generator H_I by

$$\left[\hat{S}_I\right] = \begin{vmatrix} \frac{1-N^2}{1+N^2} H_I & \frac{2}{1+N^2} H_I \\ \frac{2}{1+N^2} H_I & -\frac{1-N^2}{1+N^2} H_I \end{vmatrix}. \tag{14}$$

H_I is a Heaviside unit step defined as

$$H_I = \begin{cases} 1, & \text{on the dielectric,} \\ 0, & \text{otherwise.} \end{cases} \tag{15}$$

C. The Scattering Operator at the Interface Ω

The addition of the scattering operators $\hat{S}_M$ and

$\hat{S}_I$ enables the definition of the scattering operator $\hat{S}_\Omega$ at the interfaceΩ as

$$\left[\hat{S}_\Omega\right] = \begin{vmatrix} -H_M + \frac{1-N^2}{1+N^2} H_I & \frac{2}{1+N^2} H_I \\ \frac{2}{1+N^2} H_I & -H_M - \frac{1-N^2}{1+N^2} H_I \end{vmatrix}. \quad (16)$$

2. Reflection Operator Determination

The modes are coupled in the space domain but this is not the case in the modal domain. Each mode is reflected from the closing ends by its own reflection coefficient and the operation is done in the modal domain. To access the modal domain, FMT is used; to go back to the spatial domain, FMT^{-1} is used.

The reflection coefficient in the modal domain is given by

$$\Gamma i_{mn}^{\alpha} = \frac{1 - Z_{oi} Yi_{mn}^{\alpha}}{1 + Z_{oi} Yi_{mn}^{\alpha}}, \quad (17)$$

where Yi_{mn}^{α} is the admittance of the *mn*-th mode at the medium *i* and α stands for the modes TE or TM.

When no closing ends exist, Yi_{mn}^{α} can be calculated by [7]

$$\hat{Y}i_{mn}^{TM} = \frac{j\omega\varepsilon_o\varepsilon_{ri}}{\gamma_{mn}^{(i)}}$$
$$\hat{Y}i_{mn}^{TM} = \frac{\gamma_{mn}^{(i)}}{j\omega\mu_o}. \quad (18)$$

$\gamma_{mn}^{(i)}$ being the propagation constant of the medium *i* and it is given by

$$\gamma_{mn}^{(i)} = \sqrt{\left(\frac{2\pi m}{a}\right)^2 + \left(\frac{2\pi m}{b}\right)^2 - k_o^2 \varepsilon_{ri}}. \quad (19)$$

In (18), ε_o, ε_{ri}, and μ_o are the permittivity of the vacuum, the relative permittivity of the medium *i*, and the permeability of the vacuum, respectively, and Yi_{mn}^{α} is the admittance brought to the interface Ω.

When the structure along the z axis is terminated in a metallic wall (short circuit), the admittance seen by each mode at the interface is given by

$$Yi_{mn}^{\alpha} cc = \hat{Y}i_{mn}^{\alpha} \coth\left(\gamma_{mn}^{(i)} h_i\right), \quad (20)$$

where h_i is the substrate thickness of the medium *i*. If a termination was an open circuit (no metallic wall at the end of the medium *i*), the admittance seen by each mode at the interface is given by

$$Yi_{mn}^{\alpha} oc = \hat{Y}i_{mn}^{\alpha} \tanh\left(\gamma_{mn}^{(i)} h_i\right). \quad (21)$$

3. N-Layer FSS Problem as a Two-Media Problem

The mode admittance at the interface is seen from the equivalent medium, or medium 2 in our case, as a load brought toward this interface. In fact, the load is the mode admittance of the *N*-th layer as shown in Fig. 4. In the figure, Q_2, Q_3,⋯, $Q_{N\text{-}1}$ are two port networks of the guide of lengths h_2, h_3 , and $h_{N\text{-}1}$ and propagation constants $\gamma_{mn}^{(2)}, \gamma_{mn}^{(3)}, \cdots$, and $\gamma_{mn}^{(N-1)}$, respectively. The layer *N* ends with an open circuit and the corresponding modal admittance Y_N is given by (21).

The modal admittance seen at the interface between layers *N*-1 and *N*-2 is [8]

$$Yi_{mn\ (N-1)}^{\alpha} = \hat{Y}i_{mn\ (N-1)}^{\alpha} \left(\frac{Yi_{mn\ (N)}^{\alpha} + \hat{Y}i_{mn\ (N-1)}^{\alpha} \tanh\left(\gamma_{mn}^{(N-1)} h_{(N-1)}\right)}{\hat{Y}i_{mn\ (N-1)}^{\alpha} + Yi_{mn\ (N)}^{\alpha} \tanh\left(\gamma_{mn}^{(N-1)} h_{(N-1)}\right)} \right) \quad (22)$$

and the modal admittance seen at the interface between layers *i*-2 and *i*-1 can be calculated by

$$Yi_{mn\ (i-1)}^{\alpha} = \hat{Y}i_{mn\ (i-1)}^{\alpha} \left(\frac{Yi_{mn\ (i-2)}^{\alpha} + \hat{Y}i_{mn\ (i-1)}^{\alpha} \tanh\left(\gamma_{mn}^{(i-1)} h_{(i-1)}\right)}{\hat{Y}i_{mn\ (i-1)}^{\alpha} + Yi_{mn\ (i-2)}^{\alpha} \tanh\left(\gamma_{mn}^{(i-1)} h_{(i-1)}\right)} \right). \quad (23)$$

The modal admittance seen at the interface Ω on which the metallic patch is etched is given by the same formula as

$$Yi_{mn\ (2)}^{\alpha} = \hat{Y}i_{mn\ (2)}^{\alpha} \left(\frac{Yi_{mn\ (3)}^{\alpha} + \hat{Y}i_{mn\ (2)}^{\alpha} \tanh\left(\gamma_{mn}^{(2)} h_{(2)}\right)}{\hat{Y}i_{mn\ (2)}^{\alpha} + Yi_{mn\ (3)}^{\alpha} \tanh\left(\gamma_{mn}^{(2)} h_{(2)}\right)} \right). \quad (24)$$

The term $Yi_{mn\ (2)}^{\alpha}$ is calculated only once at the beginning of the iterations. Thus, the multilayer problem of Fig. 2 can be

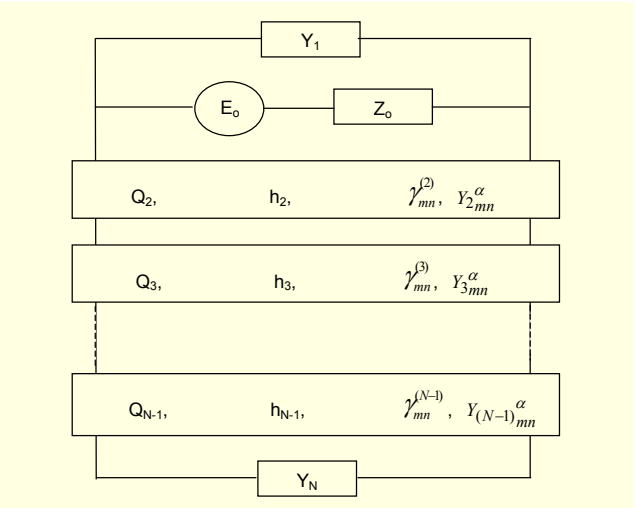

Fig. 4. Equivalent circuit of the N layers FSS unit cell.

reduced to an equivalent of the two-media problem of Fig. 3.

4. Fast Modal Transform (FMT)

The FMT/FMT^{-1} pair permits movement from the spatial domain to the modal domain and back to the spatial domain. It is summarized in the following two equations, for which the development is detailed in the appendix:

$$FMT\left(\begin{vmatrix} E_x(x,y) \\ E_y(x,y) \end{vmatrix}\right) = \begin{vmatrix} B_{mn}^{TE} \\ B_{mn}^{TM} \end{vmatrix} = \begin{vmatrix} K_{ymn} & -K_{xmn} \\ K_{xmn} & K_{ymn} \end{vmatrix} FFT2\left(\begin{vmatrix} E_x(x,y) \\ E_y(x,y) \end{vmatrix}\right),$$

$$FMT^{-1}\left(\begin{vmatrix} B_{mn}^{TE} \\ B_{mn}^{TM} \end{vmatrix}\right) = \begin{vmatrix} E_x(x,y) \\ E_y(x,y) \end{vmatrix} = FFT2^{-1}\left(\begin{vmatrix} K_{ymn} & K_{xmn} \\ -K_{xmn} & K_{ymn} \end{vmatrix} \begin{vmatrix} B_{mn}^{TE} \\ B_{mn}^{TM} \end{vmatrix}\right). \quad (25)$$

5. FSS on Anisotropic Layers

The anisotropy of the layers is taken into account in the analysis by the determination of the equivalent relative isotropic layers. When $\varepsilon_{xx}=\varepsilon_{yy}$, the parameters of this equivalent isotropic layer are given by [9]

$$\varepsilon_{req} = \sqrt{\varepsilon_{xx}\varepsilon_{zz}},$$
$$h_{eq} = h\sqrt{\frac{\varepsilon_{xx}}{\varepsilon_{zz}}}, \quad (26)$$

where h is the thickness of the anisotropic substrate.

III. Results and Discussion

The WCIP is used to analyze the rectangular FSS of a repeated structure shown in Fig. 5.

The structure consists of four layers in which the first and the last are air. Figure 6 represents the reflected power and the transmitted power obtained by the WCIP method when a normal incidence is considered. A grid of 80 by 80 pixels is used to define the interface and the results are recorded after

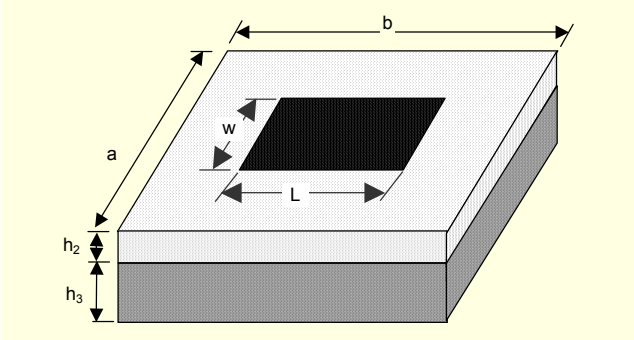

Fig. 5. Repeated unit cell in the rectangular FSS structure.

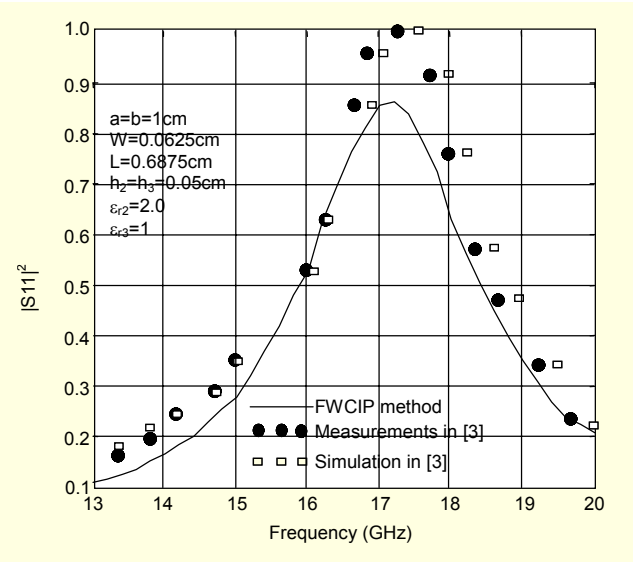

Fig. 6. Variation of the transmission power and the reflected power versus frequency.

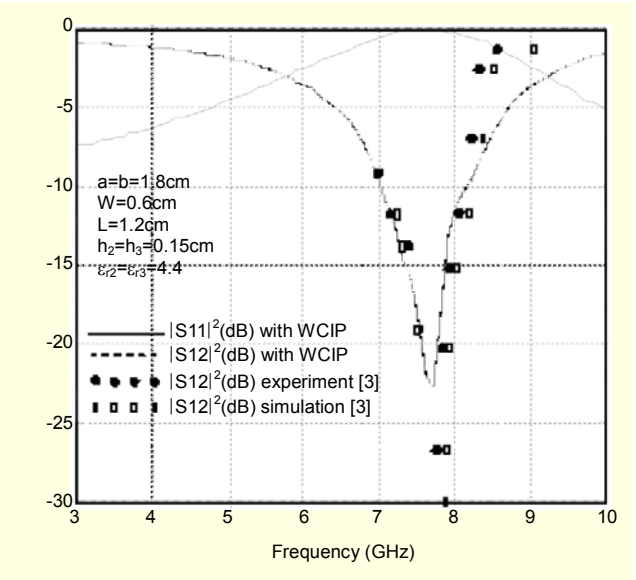

Fig. 7. Variation of the transmission power and the reflected power versus frequency on two isotropic layers.

600 iterations. As shown in Fig. 6, the structure acts as a stop band filter. Resonance occurs at about 17.3 GHz. It is clear that a good agreement with experimental results is obtained.

In Fig. 7, layers 2 and 3 are taken of the same isotropic material and of the same thickness. The numerical and measured results are plotted in the same figure. A good agreement is recorded.

Figure 8 shows the FSS of rectangular patches deposited on two anisotropic layers. A grid of 80 by 80 pixels is used and the results are recorded after 800 iterations. Resonance occurs at about 8.4 GHz compared to 8.2 GHz obtained for the same

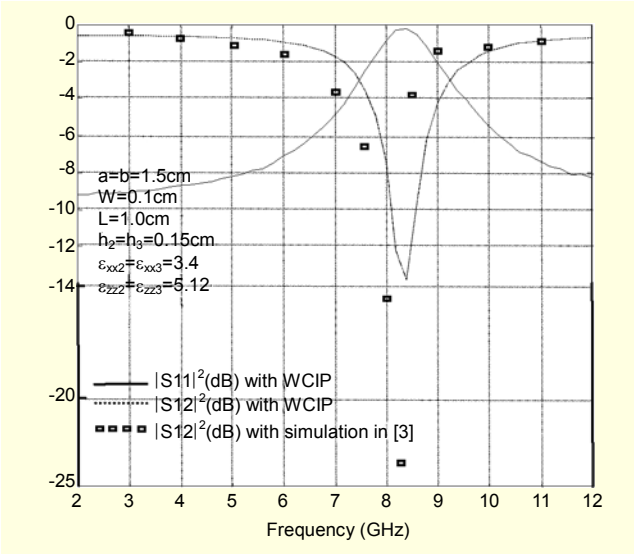

Fig. 8. Variation of transmission power and reflected power versus frequency on two anisotropic layers.

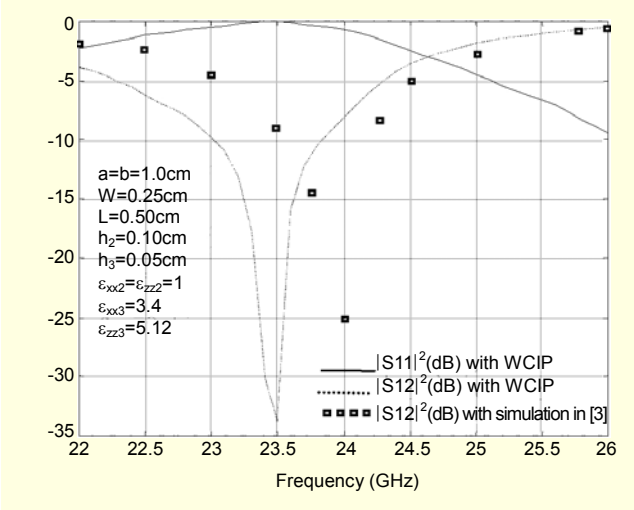

Fig. 9. Behaviour of reflected power from the FSS and transmitted power through the same FSS.

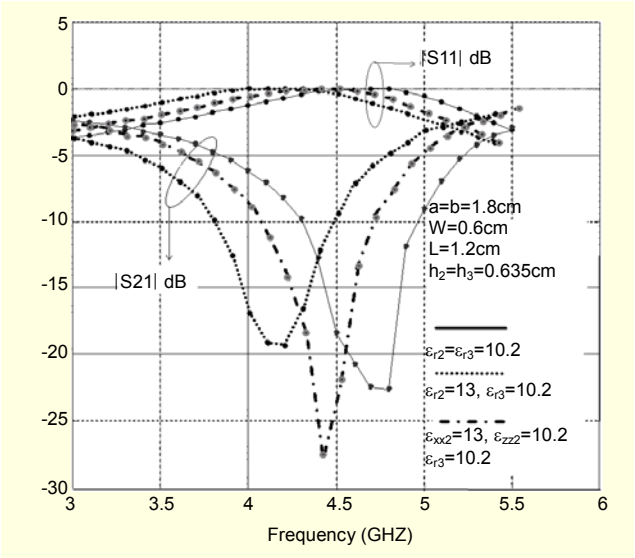

Fig. 10. Variation of transmission power and reflected power versus frequency on two dielectric layers obtained by the WCIP method.

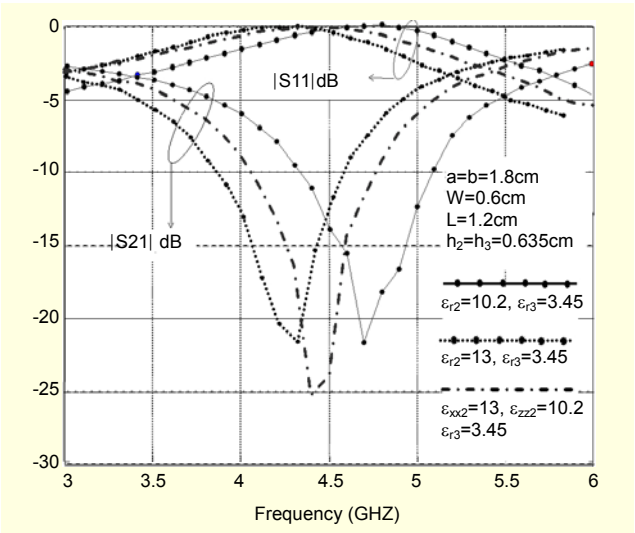

Fig. 11. Variation of transmission power and reflected power versus frequency on two dielectric layers obtained by the WCIP method.

parameters in [3].

Figure 9 represents the reflected power and the transmitted power versus frequency for a suspended FSS deposited on an anisotropic layer. Resonance is seen at 23.5 GHz.

The difference between results obtained by the WCIP method and the experimental results of reference [3] presented in Figs. 6 and 7 is due to the insufficient number of pixels used to define the interface Ω. Increasing the number of pixels leads to an improvement in the obtained results but also increases the computing time and the memory needed. Generally, anisotropic dielectrics are characterized by fewer losses compared to isotropic dielectrics.

Figures 10 and 11 show the computed transmission power and reflection power when the third layer is an isotropic Epsilam-10 and when it is isotropic pyrolitic-boron-nitride, respectively. It can be noticed that the predicted resonant frequency of the FSS when the second layer is isotropic with a relative permittivity of 13 is below the predicted resonant frequency of the same FSS when the second layer is made of an anisotropic Epsilam-10, whereas the predicted resonant frequency of the FSS when the second layer is an isotropic substrate with a relative permittivity of 10.2 is above the predicted resonant frequency of the FSS when the second layer is assumed to be an anisotropic Epsilam-10.

IV. Conclusion

A simple and efficient method for the analysis of the FSS of arbitrarily shaped conducting patches was presented. Flexible selectivity was achieved when adopting anisotropic multilayer configurations in FSS realization. By using simple relations, the multilayer problem was accounted for by the WCIP method without leading to a heavy computing time. The choice of the number of pixels used to define the interface was based on achieving a compromise between the precision of the obtained results and the time consumption. Simulated results obtained by WCIP are in good agreement with measurements and the literature. Moreover, the WCIP method holds strongly for the analysis of co-planar structures.

Appendix. FMT and FMT^{-1} Development

The transverse modes basis functions for periodic walls are given by

$$\begin{cases} f_{xmn}^{TE}(x,y) = \dfrac{n/b}{\sqrt{ab}\sqrt{(m/a)^2+(n/b)^2}} e^{-j\frac{2\pi m}{a}x} e^{-j\frac{2\pi n}{b}y}, \\ f_{ymn}^{TE}(x,y) = \dfrac{-m/a}{\sqrt{ab}\sqrt{(m/a)^2+(n/b)^2}} e^{-j\frac{2\pi m}{a}x} e^{-j\frac{2\pi n}{b}y}, \\ f_{xmn}^{TM}(x,y) = \dfrac{m/a}{\sqrt{ab}\sqrt{(m/a)^2+(n/b)^2}} e^{-j\frac{2\pi m}{a}x} e^{-j\frac{2\pi n}{b}y}, \\ f_{ymn}^{TM}(x,y) = \dfrac{n/b}{\sqrt{ab}\sqrt{(m/a)^2+(n/b)^2}} e^{-j\frac{2\pi m}{a}x} e^{-j\frac{2\pi n}{b}y}, \end{cases}$$

The electric field can be projected on these basis functions as

$$\left|E_x(x,y)\right\rangle = \sum_{m,n} B_{mn}^{TE}\left|f_{xmn}^{TE}\right\rangle + \sum_{m,n} B_{mn}^{TM}\left|f_{xmn}^{TM}\right\rangle,$$
$$\left|E_y(x,y)\right\rangle = \sum_{m,n} B_{mn}^{TE}\left|f_{ymn}^{TE}\right\rangle + \sum_{m,n} B_{mn}^{TM}\left|f_{ymn}^{TM}\right\rangle.$$

To get the benefit of the FFT algorithm, the Cartesian basis is adopted on which the electric field E is projected, leading to

$$\left|E_x(x,y)\right\rangle = \sum_{m,n} E_{xmn}\left|e^{-j\frac{2\pi m}{a}x} e^{-j\frac{2\pi n}{b}y}\right\rangle,$$
$$\left|E_y(x,y)\right\rangle = \sum_{m,n} E_{ymn}\left|e^{-j\frac{2\pi m}{a}x} e^{-j\frac{2\pi n}{b}y}\right\rangle.$$

Using the two-dimensional FFT algorithm, E_{xmn} and E_{ymn} can be obtained easily from $E_x(x,y)$ and $E_y(x,y)$, respectively.

Projecting $E_x(x,y)$ and $E_y(x,y)$ on the modal basis results in

$$\left\langle f_{xmn}^{TE} / E_x(x,y)\right\rangle = \sum_{m,n} B_{mn}^{TE}\left\langle f_{xmn}^{TE} / f_{xmn}^{TE}\right\rangle + \sum_{m,n} B_{mn}^{TM}\left\langle f_{xmn}^{TE} / f_{xmn}^{TM}\right\rangle,$$
$$\left\langle f_{ymn}^{TE} / E_y(x,y)\right\rangle = \sum_{m,n} B_{mn}^{TE}\left\langle f_{ymn}^{TE} / f_{ymn}^{TE}\right\rangle + \sum_{m,n} B_{mn}^{TM}\left\langle f_{ymn}^{TE} / f_{ymn}^{TM}\right\rangle.$$

Replacing $E_x(x,y)$ and $E_y(x,y)$ leads to

$$\sum_{m,n} E_{xmn}\left\langle f_{xmn}^{TE} / e^{-j\frac{2\pi m}{a}x} e^{-j\frac{2\pi n}{b}y}\right\rangle = \sum_{m,n} B_{mn}^{TE}\left\langle f_{xmn}^{TE} / f_{xmn}^{TE}\right\rangle + \sum_{m,n} B_{mn}^{TM}\left\langle f_{xmn}^{TE} / f_{xmn}^{TM}\right\rangle,$$
$$\sum_{m,n} E_{ymn}\left\langle f_{ymn}^{TE} / e^{-j\frac{2\pi m}{a}x} e^{-j\frac{2\pi n}{b}y}\right\rangle = \sum_{m,n} B_{mn}^{TE}\left\langle f_{ymn}^{TE} / f_{ymn}^{TE}\right\rangle + \sum_{m,n} B_{mn}^{TM}\left\langle f_{ymn}^{TE} / f_{ymn}^{TM}\right\rangle.$$

The different scalar products can be calculated and are given by

$$\left\langle f_{xmn}^{TE} / f_{xmn}^{TE}\right\rangle = \iint_S f_{xmn}^{TE\,*} f_{xmn}^{TE} dS = \frac{n^2}{b^2} k_{mn}^2,$$
$$\left\langle f_{ymn}^{TE} / f_{ymn}^{TE}\right\rangle = \iint_S f_{ymn}^{TE\,*} f_{ymn}^{TE} dS = \frac{m^2}{a^2} k_{mn}^2,$$
$$\left\langle f_{xmn}^{TE} / f_{xmn}^{TM}\right\rangle = \iint_S f_{xmn}^{TE\,*} f_{xmn}^{TM} dS = \frac{mn}{ab} k_{mn}^2,$$
$$\left\langle f_{ymn}^{TE} / f_{ymn}^{TM}\right\rangle = \iint_S f_{ymn}^{TE\,*} f_{ymn}^{TM} dS = -\frac{mn}{ab} k_{mn}^2,$$
$$\left\langle f_{xmn}^{TE} / e^{-j\frac{2\pi mx}{a}} e^{-j\frac{2\pi ny}{b}}\right\rangle = \iint_S f_{xmn}^{TE\,*} e^{-j\frac{2\pi mx}{a}} e^{-j\frac{2\pi ny}{b}} dS = \frac{n}{b} k_{mn},$$
$$\left\langle f_{ymn}^{TE} / e^{-j\frac{2\pi mx}{a}} e^{-j\frac{2\pi ny}{b}}\right\rangle = \iint_S f_{ymn}^{TE\,*} e^{-j\frac{2\pi mx}{a}} e^{-j\frac{2\pi ny}{b}} dS = \frac{-m}{a} k_{mn},$$

where

$$k_{mn} = \frac{1}{\sqrt{\dfrac{m^2}{a^2}+\dfrac{n^2}{b^2}}}.$$

Thus, E_{xmn} and E_{ymn} can be calculated by

$$E_{xmn} = \frac{n}{b} k_{mn} B_{mn}^{TE} + \frac{m}{a} k_{mn} B_{mn}^{TE},$$
$$E_{ymn} = \frac{-m}{a} k_{mn} B_{mn}^{TE} + \frac{n}{b} k_{mn} B_{mn}^{TM}.$$

Given

$$K_{xmn} = \frac{m}{a} k_{mn},$$
$$K_{ymn} = \frac{m}{b} k_{mn},$$

E_{xmn} and E_{ymn} can be written more concisely as

$$\begin{vmatrix} E_{xmn} \\ E_{ymn} \end{vmatrix} = \begin{vmatrix} K_{ymn} & K_{xmn} \\ -K_{xmn} & K_{ymn} \end{vmatrix} \begin{vmatrix} B_{mn}^{TE} \\ B_{mn}^{TM} \end{vmatrix}.$$

Hence, the transition from the modal domain to the Fourier domain (spectral domain) is obtained as a simple multiplication by the transition operator $\hat{T}^{-1}$ given as

$$\hat{T}^{-1} = \begin{vmatrix} K_{ymn} & K_{xmn} \\ -K_{xmn} & K_{ymn} \end{vmatrix}.$$

On the other hand, the transition from the Fourier domain to the modal domain can be obtained by calculation of the inverse of the transition operator $\hat{T}^{-1}$ given by

$$\hat{T} = \begin{vmatrix} K_{ymn} & -K_{xmn} \\ K_{xmn} & K_{ymn} \end{vmatrix}.$$

The amplitude of modes can be calculated using

$$\begin{vmatrix} B_{mn}^{TE} \\ B_{mn}^{TM} \end{vmatrix} = \begin{vmatrix} K_{ymn} & -K_{xmn} \\ K_{xmn} & K_{ymn} \end{vmatrix} \begin{vmatrix} E_{xmn} \\ E_{ymn} \end{vmatrix}.$$

The FMT/FMT^{-1} pair can be summarized as

$$FMT\left(\begin{vmatrix} E_x(x,y) \\ E_y(x,y) \end{vmatrix}\right) = \begin{vmatrix} B_{mn}^{TE} \\ B_{mn}^{TM} \end{vmatrix} = \begin{vmatrix} K_{ymn} & -K_{xmn} \\ K_{xmn} & K_{ymn} \end{vmatrix} FFT2\left(\begin{vmatrix} E_x(x,y) \\ E_y(x,y) \end{vmatrix}\right),$$

$$FMT^{-1}\left(\begin{vmatrix} B_{mn}^{TE} \\ B_{mn}^{TM} \end{vmatrix}\right) = \begin{vmatrix} E_x(x,y) \\ E_y(x,y) \end{vmatrix} = FFT2^{-1}\left(\begin{vmatrix} K_{ymn} & K_{xmn} \\ -K_{xmn} & K_{ymn} \end{vmatrix}\right)\left(\begin{vmatrix} B_{mn}^{TE} \\ B_{mn}^{TM} \end{vmatrix}\right).$$

For the (0,0) mode corresponding to the TEM mode, it is clear that it is supported by the periodic structure even though in the derivations this case leads to an undefined result arising from the division by zero. From the above development, two perpendicular TEM modes exist. One is to be polarized along TE modes and the other polarized along TM modes.

In the derivation of the FMT and FMT^{-1}, the electric field is taken only as an example. In fact, in the iterative method, the FMT/FMT^{-1} pair is applied to the diffracted wave B_i and the reflected wave A_i.

References

[1] Q. Gao, D.B. Yan, N.C. Yuan, and Y.Q. Fu, "Resonance of Compact Frequency Selective Surface Arrays," *Progress In Electromagnetics Research Symposium 2005*, Hangzhou, Aug. 2005, pp. 23-26.

[2] B. Monacelli, J.B. Pryor, B.A. Munk, D. Kotter, and G.D. Boreman, "Infrared Frequency Selective Surface Based on Circuit-Analog Square Loop Design," *IEEE Transactions on Antennas and Propagation*, vol. 53, no. 2, Feb. 2005, pp. 745-752.

[3] A.L.P.S. Campos, A.G. D'Assunção, and A.G. Neto, "Scattering Characteristics of FSS on Two Anisotropic Layers for Incident Co-polarized Plane Waves," *Microwave and Optical Technology Letters*, vol. 33, no. 1, Apr. 2002, pp. 57-61.

[4] R.S. N'Gongo and H. Baudrand, "Application of Wave Concept Iterative Procedure in Planar Circuits," *Recent Res. Devel. Microwave Theory and Technique*, 1999, vol. 1, pp. 187-197.

[5] T.C. Edwards, *Foundations for Microstrip Circuit Design*, John Wiley and Sons, Ltd., 1981.

[6] N. Raveu, T.P. Vuong, I. Terrasse, G.P. Piau, and H. Baudrand, "Near-Fields Evaluated with the Wave Concept Iterative Procedure Method for an e-Polarisation Plane Wave Scattered by Cylindrical Strips," *Microwave and Optical Technology Letters*, vol. 38, no. 5, Sep. 2003, pp. 403-406.

[7] R. Garcia, *Contribution a l'Etude de Circuits Planaires par une Méthode Itérative Basée sur le Concept d'Onde (F.W.C.I.P.)*, Thèse de Doctorat, Laboratoire d'électronique de LEN7, France, 2001.

[8] S. Akatimagool, *Contribution au Développement d'Outils de Simulation Electromagnétique des Circuits Planaires Multicouches*, Thèse de Doctorat, Laboratoire d'électronique de LEN7, France, 2001.

[9] M. Horno, "Calculation of Quasi-static Characteristics of Microstrip on Anisotropic Substrate Using Mapping Method," *Microwave Symposium Digest, MTT-S International*, 1980, vol. 80, no. 1, pp. 450-452.

Mohammed Titaouine was born in Batna, Algeria, in 1972. He received the electronics engineering diploma in 1995 from the INELEC (Institut National d'Electricité et d'Electronique, Boumerdes), Algeria. He received the MS degree in electronics in 1998 from the University of Sétif. He joined the Electronics Institute of the University Center of Bordj Bou-Arréridj, Algeria, in 2001. His research interests include modeling of active and passive circuits and microstrip antennas.

Alfrêdo Gomes Neto was born in João Pessoa, Brazil, in 1964. He received the BSc (1986), the MSc (1989), and DSc (1994) degrees in electrical engineering from the Federal University of Paraíba, Campina Grande, Brazil. Since 1989, he has been with the Federal Education Technological Center of Paraíba, CEFET-PB, João Pessoa, Brazil, where he was founder of the Group of Telecommunications and Applied Electromagnetism, GTEMA. During 1993 and 2005, he was a visiting researcher at the ENSEEIHT, Toulouse, France. His research interests include applied electromagnetism and numerical techniques for the design of microwave circuits and antennas.

Henry Baudrand is a Professor Emeritus at the Ecole Supérieure d'Electronique Electrotechnique Informatique, ENSEEIHT, Toulouse, France. He specializes in modeling passive and active circuits and antennas. He is the author and co-author of three books: *Introduction au calcul des éléments de circuits micoondes, Optimisation des circuits non linéaires,* and *Calcul des circuits microondes par les schémas équivalents exercices* CEPADUES Editions. He has co-authored over 100 publications in journals and 250 contributions to international conferences. He is a Fellow Member of IEEE Society, a Member of "Electromagnetism Academy" and a Senior Member of IEE society. He was the President of URSI France commision B for 6 years (1993-1999), and the President of the IEEE-MTT-ED French chapter. He was awarded Officier des Palmes académiques, and Director Honoris causa of lasi University.

Farid Djahli was born in Sétif, Algeria, on May 25, 1955. He received the electronics engineering diploma in 1981 and the MS degree in electronics in 1985, from the ENPA (Ecole Nationale Polytechnique d'Alger). In 1992, he received the PhD in microelectronics from LPM of INSA, Lyon (Laboratoire de Physique de la Matière, Institut National des Sciences Appliquées), France. He worked on the modeling of the degradation of MOSFETs using different techniques of characterization, especially the charge pumping technique. He joined the Electronics Institute of the University of Sétif, Algeria, in 1992, where he currently works as a Professor. In addition to microelectronics, his research interests include MMIC circuits, modeling of microstrip discontinuities, and microstrip antennas. He is the author and the co-author of more than 60 scientific papers.